VOL. 13, NO. 11, JUNE 2018 ISSN 1819-6608
ARPN Journal of Engineering and Applied Sciences

www.arpnjournals.com

# SYNTHETIC SEISMOGRAMS WITH THE RESERVOIR PARAMETER EFFECT

Sismanto
Geophysics Division, Department of Physics, Gadjah Mada University, Yogyakarta, Indonesia
E-Mail: sismanto@ugm.ac.id

**ABSTRACT**

In one-dimension (1D), we build synthetic seismograms to visualize the effect of reservoir parameter based on Ganley method. The effects such as absorption, dispersion, and attenuation are combined in the complex wave number. The attenuation effects are calculated from the wave number of Biot's equation, and the Futterman's absorption-dispersion equations are used. The Geertsma and Smit relationship is implemented to the model permeability determining. The reservoir of a porous medium has a significant effect on the frequency dependence of attenuation even in the frequency content for a surface seismic wave. The frequency spectrums of propagation wave in a porous medium can show the frequency-shift that caused by reservoir attenuation system, and the synthetic seismograms may be used to test any inversion method of reservoir parameters.

**Keywords:** synthetics seismogram, absorption, dispersion, attenuation.

## INTRODUCTION

Ganley already designed a method for calculating synthetic seismogram of vertical seismic profiles (VSP), which included the effects of absorption and dispersion [1]. The absorption model was the usual model of exponential decay of amplitude with distance. According to Biot theory [2], fast and slow compressional (P) waves are excited and there is a mode conversion at the interface. Turgut and Yamamoto [3] developed a one-dimensional (1D) model of VSP, which includes mode conversion through slow P waves as an energy loss mechanism based on Ganley [1], which covered the effect of dispersion and attenuation of reservoir parameters such as porosity and permeability for marine sediment. Geophysicists believe that the reservoir parameters affect the seismic wave and elastics characters. Synthetic VSP seismograms with attenuation had been constructed by Dong and Margrave [4], they method based upon the wavefield extrapolation theory for plane waves in a flat layered model with constant-Q attenuation. Most theoretical and experimental researchers prove that there is a close relationship in those parameters [5] and [6]. Best *et al.*, [7] studied about the relationships between the velocities, attenuations, and petrophysical properties of reservoir sedimentary rocks. Best, [8] investigated the effect of pressure on ultrasonic velocity and attenuation in near-surface sedimentary rocks. Whereas, the P wave velocity and attenuation at ultrasonic and sonic frequencies in near-surface sedimentary rocks had been reviewed by Best and Sams [9]. The usage of seismic attenuation to indicate saturation in hydrocarbon reservoirs was studied theoretically and modelling approach by Raji [10] and Sismanto[6].

The aim of this work is to construct 1D synthetic seismograms in horizontal and vertical seismic profiling (HSP and VSP) by associating the effect of absorption-dispersion from Ganley and dispersion-attenuation with reservoir parameter from Biot. The synthetic seismograms that are obtained can be enforced to check and test any inversion of permeability and saturation estimation method.

## METHODOLOGY

According to Biot [2], the bases of two wave equations for a fluid-saturated porous media are;

$$\mu\nabla^2\vec{u} + (\overline{H}-\mu)\nabla\theta - C\nabla\varsigma_p = \rho\frac{\partial^2\vec{u}}{\partial t^2} - \rho_f\frac{\partial^2\vec{V}}{\partial t^2}, \quad (1)$$

$$C\nabla\theta - M\nabla\varsigma_p = \rho_f\frac{\partial^2\vec{u}}{\partial t^2} - m\frac{\partial^2\vec{V}}{\partial t^2} - \frac{\eta}{k_p}\frac{\partial\vec{V}}{\partial t}. \quad (2)$$

in which: $\vec{u}$ is the frame displacement vector, $\vec{V}$ is the seepage displacement vector; $\theta$ = div $\vec{u}$, $\varsigma_p$ = div $\vec{V}$, $\rho$ is the bulk density $[\rho = (1-\phi)\rho_r + \phi\rho_f]$, $\rho_r$ is the density of grain, $\rho_f$ is the density of fluid, $\phi$ is the porosity, $\eta$ is the viscosity of fluid, and is $k_p$ the coefficient of permeability. $\overline{H}$, $C$, and $M$ are Biot's elastic moduli, $\mu$ is the shear modulus, and $m$ is the virtual mass expressed as $m = \alpha\rho_f/\phi$, $\alpha = 1.25$ [11]. The Biot elastic modulus expressed by the following relations,

$$\overline{H} = \frac{(K_r - K_b)^2}{(D_r - K_b)} + K_b + \tfrac{4}{3}\mu, \quad (3a)$$

$$C = \frac{K_r(K_r - K_b)}{D_r - K_b}, \quad (3b)$$

$$M = \frac{K_r^2}{D_r - K_b}, \quad (3c)$$

$$D_r = K_r\left[1 + \phi\left(\frac{K_r}{K_f} - 1\right)\right]. \quad (3d)$$

where $K_r$ is the bulk modulus of the grain, $K_f$ is the bulk modulus of the fluid in the pores, and $K_b$ is the bulk

modulus of the skeletal frame. According to Turgut and Yamamoto [11] the porosity and bulk modulus of skeletal frame $K_b$ in Equation (3) is,

$$\phi = \frac{K_f(K_r - K)}{(K_r - K_f)(K - K_b)}, \text{ and} \quad (4a)$$

$$K_b = \left(\frac{2\sigma}{1-2\sigma} + \tfrac{2}{3}\right)\mu \cdot \quad (4b)$$

In term of velocity, the bulk modulus $K$, shear modulus$\mu$, and Poisson's ratio $\sigma$ of medium are,

$$K = \rho\left(V_p^2 - \frac{4}{3}V_s^2\right), \quad (5a)$$

$$\mu = \rho V_s^2, \quad (5b)$$

$$\sigma = \frac{3K - 2\mu}{2(3K + \mu)} \quad (5c)$$

For 1-D case in harmonic waves, the velocity solutions of Eqs. (1) and (2) are,

$$\frac{1}{\hat{V}_p^2} = \frac{-(\overline{H}\hat{q} + M\rho - 2C\rho_f) \pm \sqrt{(\overline{H}\hat{q} + M\rho - 2C\rho_f)^2 - 4(C^2 - M\overline{H})(\rho_f^2 - \rho\hat{q})}}{2(C^2 - M\overline{H})}, \quad (6)$$

and $$\frac{1}{\hat{V}_s^2} = \frac{\hat{q}\rho - \rho_f^2}{\hat{q}\mu}, \quad (7)$$

where $$\hat{q} = \frac{\alpha\rho_f}{\phi} - i\frac{\eta}{\omega k_p} \cdot \quad (8)$$

The velocity is a complex number, the real and imaginary part of which are the velocity and attenuation of wave propagation in the medium respectively. Geertsma and Smit [12] showed that for most marine sediment the following inequality,

$$\frac{(-\overline{H}q - M\rho + 2C\rho_f)}{2(C^2 - \overline{H}M)^{1/2}} \rangle\rangle 1 \text{ is valid.} \quad (9)$$

Considering this inequality, the Equation (6) can be approximated as,

$$[\hat{V}_p^2]^{-1} \approx (\rho\hat{q} - \rho_f^2)/(\overline{H}\hat{q} + M\rho - 2C\rho_f) \text{ or} \quad (10)$$

$$\hat{l}^2 \approx \omega^2(\rho\hat{q} - \rho_f^2)/(\overline{H}\hat{q} + M\rho - 2C\rho_f) \quad (11)$$

$\tilde{l}_i(\omega) = \omega/\tilde{V}_i(\omega)$ is the wave number as a frequency function and the frequency-dependent phase velocity of the wave in the medium and the function of the elasticity and reservoir parameters (porosity, permeability, viscosity). For unconsolidated rock sediments are,

$$\tilde{l}_i(\omega) = \omega\sqrt{\frac{(\rho\tilde{q} - \rho_f^2)}{\overline{H}\tilde{q} + M\rho - 2C\rho_f}} \quad (12)$$

with, $\overline{H}$, M, and C are Biot's elastic constants given by Equation (3) and $\tilde{q}$ are complex numbers given by Equation (8).

From definition of intrinsic attenuation for a high quality factor $Q$, Turgut and Yamamoto [11] derive the velocity for zero and high frequency such as

$$V_0^2 = \frac{\overline{H}}{\rho}, \text{ for } \omega \to 0, \text{ and} \quad (13a)$$

$$V_\infty^2 = \left[\frac{(\overline{H}m + M\rho - 2C\rho_f)}{(\rho m - \rho_f^2)}\right] \text{for } \omega \to \infty. \quad (13b)$$

Castagna *et al,* [13] and Mavko *et al*, [5] empirically made a relationship of $V_s$-$V_p$ in polynomial form for each lithology with the coefficient or constant are summarized in Tabel-1, such as;

$$V_s = a_2V_p^2 + a_1V_p + a_o \text{ (km/s)} \quad (14)$$

Whereas the relationship of velocity $V_p$ (km/s) to bulk density $\rho_b$ (g/cm$^3$) empirically in polynomial by Castagna *et al,* [13] as;

$$\rho_b = aV_p^2 + bV_p + c \quad (15)$$

The constants are shown in Tabel-2.

The permeability values contained in the seismogram can be estimated based on Geertsma and Smit [12];

$$k_p = \frac{\Phi\eta}{2\pi\rho_f}\frac{1}{\sqrt{\frac{V_\infty^4 - V_p^2V_\infty^2}{V_p^2V_o^2 - V_o^4}}} \quad (16)$$

Thus, by defining the $V_p$, $K_r$, $K_b$, $K_f$, $\eta$, $\rho_f$, and $\rho_r$ of model, then all elastic parameters and reservoir parameters will be estimated by means of Equation (3), (4), (5), (14), (15) and (16).

**Table-1.** The polynomial constant of $V_p$-$V_s$ relationship with regression coefficient by Castagna *et al*, [13].

| Lithologi | $a_2$ | $a_1$ | $a_o$ | $V_p$ (km/s) | $R^2$ |
|---|---|---|---|---|---|
| sandstone | 0 | 0,80416 | -0,85588 | 2 – 6 | 0,98352 |
| limestone | -0,05508 | 1,01677 | -1,03049 | 1,5 – 6 | 0,99096 |
| dolomite | 0 | 0,58321 | -0,07775 | 4,5 – 6,4 | 0,87444 |
| shale | 0 | 0,76969 | -0,86735 | 1,5 – 5 | 0,97939 |

**Table-2.** The polynomial constant of $V_p$- $\rho$ relationship with velocity range by Castagna *et al,* [13].

| Lithologi | $a$ | $b$ | $c$ | $V_p$ (km/s) |
|---|---|---|---|---|
| shale | -0,0261 | 0,373 | 1,458 | 1,5 – 5 |
| sandstone | -0,0115 | 0,261 | 1,515 | 1,5 – 6 |
| limestone | -0,0296 | 0,461 | 0,963 | 3,5 – 6,4 |
| dolomite | -0,0235 | 0,390 | 1,242 | 4,5 – 7,1 |
| anhydrite | -0,0203 | 0,321 | 1,732 | 4,6 – 7,4 |

## SYNTHETIC SEISMOGRAM

Suppose there are two horizontal layers and if $D_i(\omega)$ is the down-waves frequency spectrum at the top layer $i$, the wave moves downward on layer $i$ at the bottom as given in Figure-1, may be provided by,

$$D'_i(\omega) = D_i(\omega) e^{-\alpha_z d'_i} e^{-id'_i \tilde{l}_i(\omega)} \quad (17)$$

where $d'_i$ is the thickness (for the zero offset) or the length of the wave path inside the layer $i$,

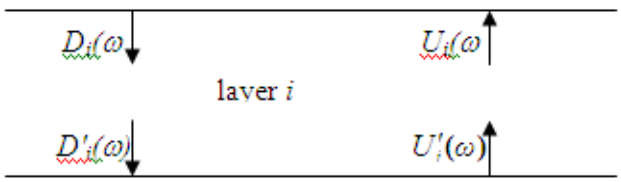


**Figure-1.** The relationship between the waves propagates from the top to down and from the bottom to up on the same layer.

The term of $e^{-\alpha_z d'_i}$ is the attenuation factor of wave energy lost (effect of dispersion and the absorption), when the wave propagates from top to bottom in layer $i$. The form $e^{-i\, d'_i \tilde{l}_i(\omega)}$ is the delay time in the wave propagation from top to bottom in the layer $i$ and attenuation due to elastic and reservoir parameters such as by porosity and permeability. For the next calculation $\tilde{l}_i(\omega)$ is taken only real part is expressed as $l_i(\omega)$.

By the same analogy $U'_i(\omega)$ which is the up-going wave spectrum from bottom to upward in layer $i$, which is associated with the up-going wave spectrum above $U_i(\omega)$ which is given by the relationship of,

$$U_i(\omega) = U'_i(\omega) e^{-\alpha_z d'_i} e^{-id'_i \tilde{l}_i(\omega)} \quad (18)$$

The boundary plane in Figure-2, the up-going wave $U'_i(\omega)$ is derived from two wave parts i.e., the transmission wave $U_{i+1}$ and the reflected wave from $D'_i$, so that it can be written as;

$$U'_i = R_i D'_i + T'_i U_{i+1} \quad (19)$$

$R_i$ is the reflection coefficient of the boundary $i$ for the incident wave or down-going wave and $T'_i$ is the transmission coefficient on the boundary $i$ for the up-going wave from the bottom.

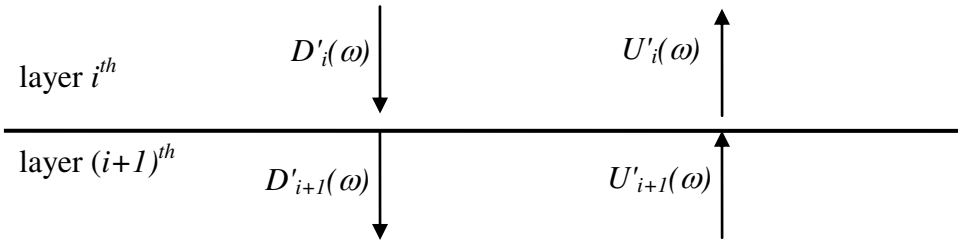


**Figure-2.** The relationship between up-going and down-going waves on a boundary plane.

As shown in Figure-2 we can also get the $D_{i+1}$ wave spectrum derived from the reflection part of the $U_{i+1}$ wave and the spectrum transmission wave part of $D_i'$ so that

$$D_{i+1} = T_i D_i' + R_i' U_{i+1} \quad (20)$$

where $R_i'$ is the coefficient on boundary *i* for the up-going wave, and $T_i$ is the transmission coefficient for the down-goingwave, and the relationship of the coefficient is,

$$1 + R = T, \quad (21)$$

and the reflection *R* and transmission *T* coefficient are,

$$R(\omega) = \frac{\rho_1 V_1(\omega) - \rho_2 V_2(\omega)}{\rho_1 V_1(\omega) + \rho_2 V_2(\omega)} = \frac{\rho_1 l_2(\omega) - \rho_2 l_1(\omega)}{\rho_1 l_2(\omega) + \rho_2 l_1(\omega)}, \quad (22)$$

and

$$T(\omega) = \frac{2\rho_1 V_1(\omega)}{\rho_1 V_1(\omega) + \rho_2 V_2(\omega)} = \frac{2\rho_1 l_2(\omega)}{\rho_1 l_2(\omega) + \rho_2 l_1(\omega)} \quad (23)$$

then it can be obtained, $D_i' = \frac{1}{T_i}\left[D_{i+1} + R_i U_{i+1}\right]$, (24)

and

$$U_i' = \frac{1}{T_i}\left[R_i D_{i+1} + U_{i+1}\right]. \quad (25)$$

The combination of Equations (24) and (25) with Equations (17) and (18) will give

$$D_i = \frac{e^{\alpha_z d_i'} e^{i d_i' l_i(\omega)}}{T_i}\left(D_{i+1} + R_i U_{i+1}\right) \quad (26)$$

$$U_i = \frac{e^{-\alpha_z d_i'} e^{-i d_i' l_i(\omega)}}{T_i}\left(R_i D_{i+1} + U_{i+1}\right) \quad (27)$$

Which in the matrix form can be written as,

$$\begin{bmatrix} D_i \\ U_i \end{bmatrix} = A_i \begin{bmatrix} D_{i+1} \\ U_{i+1} \end{bmatrix} \quad (28)$$

where the matrix $A_i$ is,

$$A_i(\omega) = \frac{1}{T_i}\begin{bmatrix} e^{\alpha_z d_i'} e^{i d_i' l_i(\omega)} & R_i e^{\alpha_z d_i'} e^{i d_i' l_i(\omega)} \\ R_i e^{-\alpha_z d_i'} e^{-i d_i' l_i(\omega)} & e^{-\alpha_z d_i'} e^{-i d_i' l_i(\omega)} \end{bmatrix} \quad (29)$$

For the *n* layer model, the up-going and down-going waves inside the first layer ($i = 1$) can be considered to be on a half-sphere medium. Thus below the $n^{th}$ layer, by applying Equation (28)) we can find the general Equation as,

$$\begin{bmatrix} D_1(\omega) \\ U_1(\omega) \end{bmatrix} = A_1(\omega), A_2(\omega), \ldots A_n(\omega) \begin{bmatrix} D_{i+1}(\omega) \\ U_{i+1}(\omega) \end{bmatrix} \quad (30)$$

If the input is a down-going wave in the form of a spike pulse at time $t = 0$, on the surface, the total down-going wave in the first layer will consist of a spike pulse added by the up-going wave of reflection on the final surface. If $R_0$ is the surface reflection coefficient for the up-going wave of the first layer, then $-R_0$ is the surface reflection coefficient for the up-going wave inside the first layer, so;

$$D_1(\omega) = 1 - R_0 U_1(\omega) \quad (31)$$

The Equation (31) is the total down-going wave in the top layer, since no other wave energy input from the model above it. If the base layer or layer to $n + 1$ is also a half-sphere medium, then no up-going wave inside the layer, since there is no source of wave energy in the layer and no reflected down-going waves, so;

$$U_{n+1}(\omega) = 0 \quad (32)$$

Substitute Equations (31) and (32) into Equation (30), so that it will give a relationship of

$$\begin{bmatrix} 1 - R_0 U_1(\omega) \\ U_1(\omega) \end{bmatrix} = A_1(\omega), A_2(\omega), \ldots A_n(\omega) \begin{bmatrix} D_{i+1}(\omega) \\ 0 \end{bmatrix} \quad (33)$$

In Equation (33) there are two Equations with two unknowns, $U_1(\omega)$ and $D_{n+1}(\omega)$, so they can be solved. $U_1(\omega)$ represents the Fourier transform of the up-going wave in layer *1,* and $D_{n+1}(\omega)$ is the Fourier transform of the down-going wave in the layer $n + 1$. If $X(\omega)$ is a Fourier transform of the synthetic seismogram on the surface given by $U_1(\omega) + D_1(\omega)$, then

$$X(\omega) = (1 - R_0) U_1(\omega) + 1 \quad (34)$$

Therefore, it is possible to design a number of layers to make the Fourier synthetic seismogram transformation on the surface for the initial wave in the form of spikes on the surface. The Fourier transform of the spike downward waveform when multiplied by the Fourier transform of the wavelet, will result in a wavelet going-down input (not a spike anymore). The thickness $d_i'$ which is also the length of the optical wave propagation path is adjusted by its optical wave path geometry for surface seismic or reflection seismic. For VSP configuration the transmission wave can be used the layer thickness. As for the path reflected wave in the HSP can be calculated from the geometric configuration.

For the construction of synthetic signal, a Ricker wavelet signal is used in the frequency domain as defined as,

$$W(\omega) = \omega^2 e^{-\omega^2/\omega_0^2} \quad (35)$$

where $\omega_0$ is the dominant frequency.

Futterman's third absorption-dispersion pair will be implemented for absorption effect [14]. In this model the absorption coefficient $\alpha_x$ is

$$\alpha_x = \omega/[2V(\omega)Q(\omega)], \quad (36)$$

$V$ and $Q$ are the velocity and quality factor of the model. When $\omega = 0$, it means that there is no dispersion effect, then the phase velocity will be same as the velocity of the model.

In modeling, the spectrum of down-going wave $D_i(\omega)$ at the top layer of $i$ and the down going wave at the bottom of layer $i$, $D_i'(\omega)$ is related by $D_i'(\omega) = D_i(\omega)e^{-\alpha_x d_i} e^{-id_i\hat{l}_i(\omega)}$ in which $d_i$ is a path of the seismic wave in the medium, especially for HSP modeling. In VSP modeling, the seismic wave path can use the thickness of the $i^{th}$ layer model. The wave number is complex in the $i^{th}$ layer that depends on the frequency and complex phase velocity. The term $\exp(-\alpha_x d_i)$ represents the energy loss due to absorption as the wave propagates from the top to the bottom of the $i^{th}$ layer. We use the term $\exp[-id_i l(\omega)]$ as the time delay, absorption, dispersion, and attenuation of the $i$th layer due to the elastics and reservoir parameters, such as density, porosity, bulk modulus, and permeability via the complex wave number as defined in Equation (11). Therefore, the synthetic seismograms cover reservoir, elastics, and wave parameters. The permeability of the model depended on those parameters are proposed by Geertsma and Smit [12]. The relationships of the permeability to the velocity and frequency for sandstone type are illustrated in Figure-3 and Figure-4, respectively. Those figures are showed that for higher frequency the velocity dependency is not relatively significant to the permeability. Otherwise, the permeability is strongly influenced by frequency.

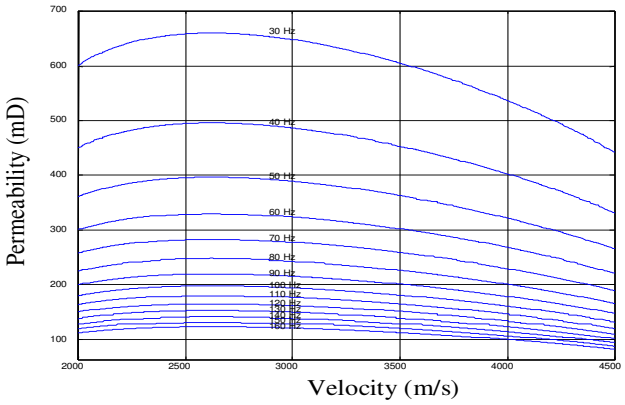


**Figure-3.** The theoretical relationship of the permeability to the velocity of sandstone type. It is showed that for higher frequency the velocity dependency is not significant to the permeability.

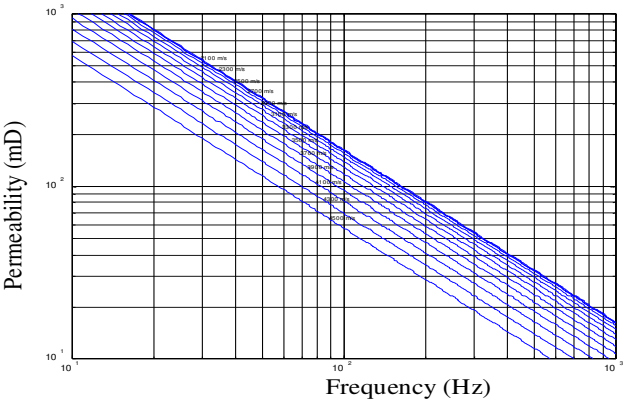


**Figure-4.** The relationship of the permeability to the frequency for sandstone type. The relationship shows that the permeability is strongly influenced by frequency.

The basic rock properties of marine sediment that used to construct HSP and VSP synthetic seismograms are based on Turgut and Yamamoto [11] such as kinematics viscosity of pure fluid ($\eta$ =1.0x10$^{-6}$ m$^2$/s), bulk modulus of fluid ($K_f$ = 2.3 x 10$^9$ N/m$^2$), bulk modulus of grain ($K_r$ = 3.6 x 10$^{10}$ N/m$^2$), density of fluid ($\rho_f$ = 1.0 x 10$^3$ kg/m$^3$), and density of grain ($\rho_r$ = 2.65 x 10$^3$ kg/m$^3$). While velocity ($V_p$) of the P wave is obtained from the geological model, and the S wave velocity ($V_s$) and density ($\rho$) are estimated by empirical Equations [13]. Then, the bulk modulus of skeletal frame and porosity are estimated by Eqs.(4) and (5), Biot's elasticity parameters are determined by Equation(3), and the velocity of $V_o$ and $V_\infty$ are calculated by Equation(13).

## NUMERICAL RESULTS OF HSP SYNTHETIC SEISMOGRAMS

A two-layer model uses the thickness of the first layer of 150 m and receiver interval is 20 m. From those rock and wave parameters, the other physical properties can be calculated. The results are used to construct the synthetic seismogram of a two-layer model, which is shown in Figure-5. The model uses a sandstone velocity

$V_{p1}$ of 3000 m/s over limestone $V_{p2}$ of 4000 m/s. The Ricker wavelet frequency is 70 hertz. Figure-6 is the frequency spectrum of the synthetic seismogram events of Figure-5. The spectrum shows that there is strongly frequency shift and amplitude attenuation, especially in the (10-70) Hz. The frequency content is affected by the attenuation system of the medium.

The synthetic seismogram of poroelastic waves for a three-layer model is presented in Figure-7, and for a four-layer model is presented in Figure-8. Due to the reservoir parameters are place together as an attenuation system of rock. On those synthetic seismograms, the effect of attenuation and dispersion change the amplitude, frequency, and phase significantly. Hence, the signals are attenuated strongly as a function of reservoir parameter besides the frequency and the distance effect. The synthetic seismograms that are obtained can be implemented to check and any inversion of permeability estimation method.


**Figure-5.** A synthetic seismograms of poroelastic waves in two-layer models of seismic reflection. The model uses a velocity $V_{p1}$ of 3000 m/s (sandstone, 150 m) over the limestone $V_{p2}$ of 4000 m/s. A Ricker wavelet frequency is 70 hertz.

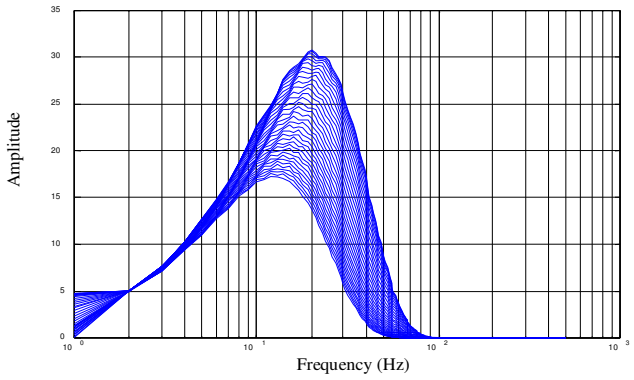


**Figure-6.** The frequency spectrum of the synthetic seismogram events of Figure-5.The spectrum shows some frequency shift and amplitude attenuation, especially in the (10-70)Hz. The frequency content is affected by the attenuation system of the medium.

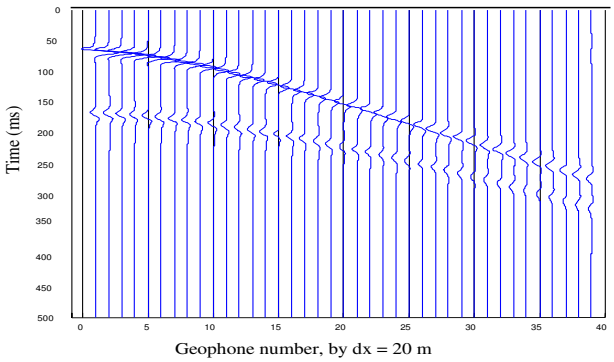


**Figure-7.** A synthetic seismograms of poroelastic waves in the three-layer model. The first layer velocity of sandstone ($V_{p1}$ is 3000 m/s) the second layer velocity of dolomite ($V_{p2}$ is 3500 m/s) and the last layer is limestone ($V_{p3}$ of 4000 m/s) are used. The Ricker's wavelet frequency is 70 hertz. The thickness of the first and second layer and the receiver interval are 100 m, 150 m, and 20 m respectively.

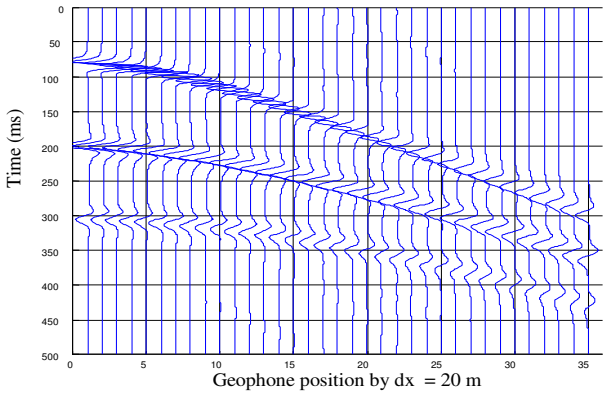


**Figure-8.** A synthetic seismograms of poroelastic waves in four-layer model. The first layer velocity of shaley-sandstone (100 m), ($V_{p1}$ is 2500 m/s) the second layer velocity of sandstone (150 m) ($V_{p2}$ is 3000 m/s) the third layer velocity of dolomite (100 m) ($V_{p2}$ is 3500 m/s) and the last layer is limestone $V_{p3}$ of 4000 m/s are used. The Ricker's wavelet frequency is 70 hertz.

## NUMERICAL RESULTS OF VSP SYNTHETIC SEISMOGRAMS

Parameters of each layer of the VSP model are velocity of 2.500, 4.000, and 5.500 m/s, density by empirical $V_p$-$\rho$ curve of 2.096, 2.426, and 2.603 kg/m$^3$, quality factor of 50, 100, and 150, thickness of 150 m, 100 m, and infinite, and the Ricker frequency is 70 Hz. The numerical synthetic seismograms of VSP for elastic medium (no attenuation) and the spectra of the frequency are presented in Figure-9 and Figure-10. It seems that the amplitude decreases and a shift of frequency do not occur. Meanwhile, the synthetic seismograms for non-elastic medium (it means just $\alpha$ an attenuation), and the spectra of the frequency are shown in Figure-11 and Figure-12. It shows that the amplitude decreases and there is a small shift in frequency. But, for poroelastic medium (with a reservoir and an attenuation $\alpha$) presented in Figure-13 and

Figure-14, the amplitude and frequency are significantly shifted. It means that the reservoir parameter effect can be visualized, and the permeability of reservoir is kept.

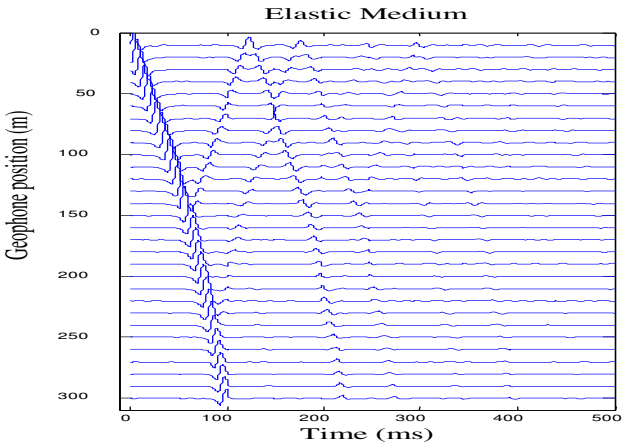


**Figure-9.** A synthetic seismograms of VSP for elastic medium (no attenuation).

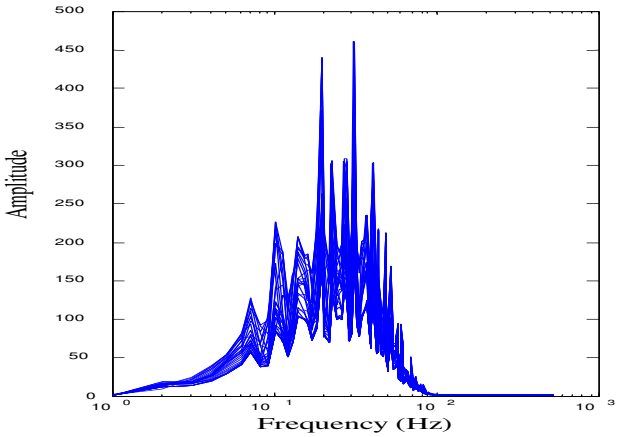


**Figure-10.** The spectra of the frequency contain all traces. It shows that the amplitude decreases and there is no any shift in frequency.

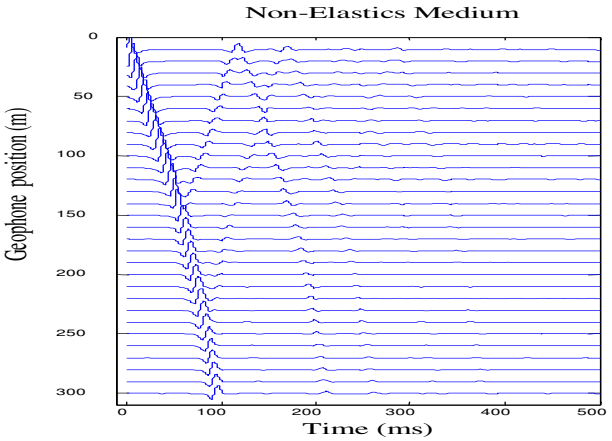


**Figure-11.** A synthetic seismograms of VSP for non-elastic medium (with attenuation).

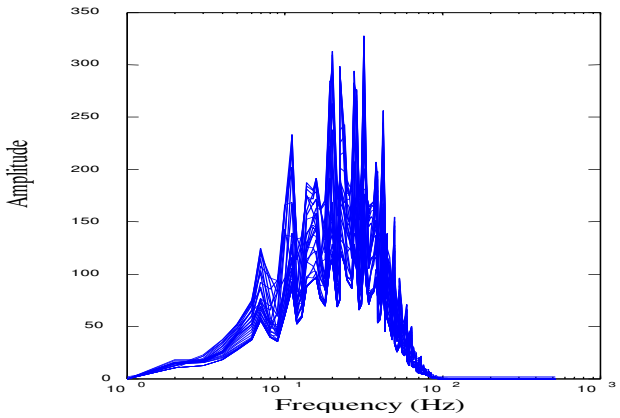


**Fugure-12.** The spectra of the frequency contain all traces. It shows amplitude decrease and small frequency-shift.

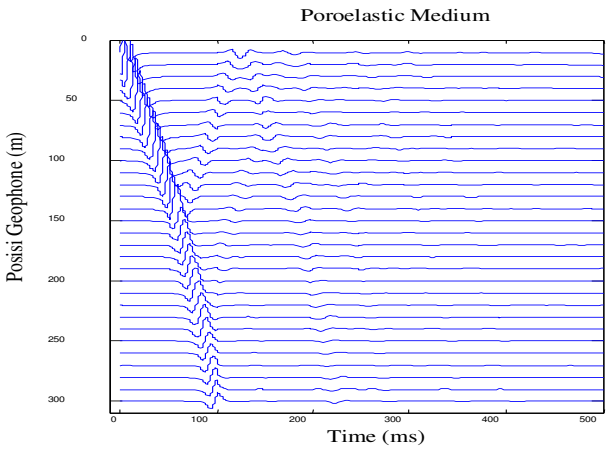


**Figure-13.** A synthetic seismograms of VSP for poroelastic medium (with attenuation).

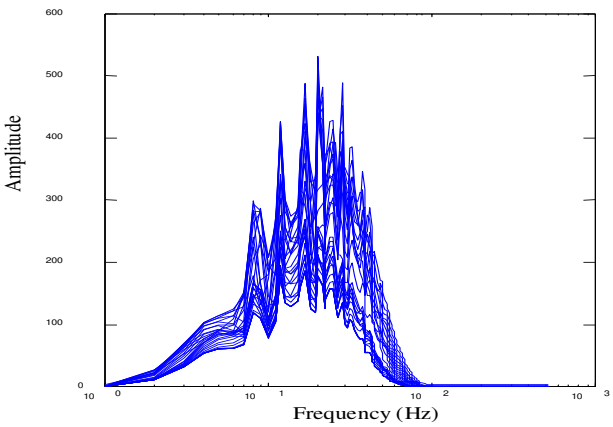


**Figure-14.** The spectra of the frequency contain all traces. It shows amplitude decrease and significant frequency-shift.

## CONCLUSIONS

The frequency spectrums of 1D synthetic seismogram in horizontal and vertical seismic profiling are able to show the frequency shift that is caused by reservoir

attenuation system. The reservoir of a porous medium has a significant effect on the frequency dependence of attenuation even in the low-frequency range relevant for surface seismic. The synthetic seismograms can be used to test any inversion method of reservoir parameters.

**ACKNOWLEDGEMENTS**

We gratefully acknowledge the invaluable support of QUE project of Geophysics Study Program of Gadjah Mada University for financial support.

**REFERENCES**

[1] D.C. Ganley. 1981. A method for calculating synthetic seismograms which include the effect of absorption and dispersion. Geophysics. 46, pp. 1100-1107.

[2] M.A. Biot. 1956. Theory of propagation of elastic waves in a fluid-saturated porous solid, J. Acous. Soc. Am. 28, pp. 168-191.

[3] A. Turgut and T. Yamamoto. 1988. Synthetic seismo-grams for marine sediments and determination of porosity and permeability. Geophysics. 53, pp.1056-1067.

[4] L. Dong and Gary F. Margrave. 2003. Synthetic VSP seismograms with attenuation. CREWES Research Report. 15: 1-12.

[5] G. Mavko, T. Mukerji and J. Dvorkin. 1998. The rocks physics handbook: Tool for seismic analysis in porous media, Cambridge Univ. Press, USA: 104.

[6] Sismanto. 2016. A New Approximation of Water Saturation Estimation Based on Vertical Seismic Profiling Data. Int. Journal of Engineering Research and Applications. 6(1, Part - 4): 49-52.

[7] A.I. Best, C. McCann, and J. Sothcott. 1994. The relationships between the velocities, attenuations, and petrophysical properties of reservoir sedimentary rocks. Geophysical Prospecting. 42, p.151-178.

[8] A.I. Best. 1997. The effect of pressure on ultrasonic velocity and attenuation in near-surface sedimentary rocks. Geophysical Prospecting. 45, pp. 345-364.

[9] A.I. Best and M.S. Sams. 1997. Compressional wave velocity and attenuation at ultrasonic and sonic frequencies in near-surface sedimentary rocks. Geophysical Prospecting. 45, pp. 327-344.

[10] W.O. Raji. 2013. The use of seismic attenuation to indicate saturation in hydrocarbon reservoirs: Theoretical study and modelling approach. Advances in Applied Science Research. 4(2): 45-53.

[11] A. Turgut and T. Yamamoto. 1990. Measurements of acoustic wave velocities and attenuation in marine sediments. J. Acoust. Soc. Am. 87, pp. 2376-2383.

[12] J. Geertsma and D.C. Smit. 1961. Some aspect of elastic wave propagation in fluid saturated porous solid. Geophysics. 26, pp. 169-181.

[13] J.P. Castagna, M.L. Batzle and T.K. Kan. 1993. Rock physics - The link between rock properties and AVO response, in Offset-Dependent Reflectivity-Theory and Practice of AVO Analysis, in J.P. Castagna and Backus. 8, pp. 3-36.

[14] W. I. Futterman. 1962. Dispersive body waves. Journ. Geoph. Res. 67, pp. 5279-5291.